



Independent $^{40}\text{Ar}/^{39}\text{Ar}$ and ^{14}C age constraints on the last five glacial terminations from the aggradational successions of the Tiber River, Rome (Italy)



F. Marra^{a,*}, E.J. Rohling^{b,c}, F. Florindo^a, B. Jicha^d, S. Nomade^e, A. Pereira^{e,f,g,h}, P.R. Renne^{i,j}

^a Istituto Nazionale di Geofisica e Vulcanologia, Via di Vigna Murata 605, 00143 Roma, Italy

^b Research School of Earth Sciences, The Australian National University, Canberra, ACT 2601, Australia

^c Ocean and Earth Science, University of Southampton, National Oceanography Centre, Southampton SO143ZH, UK

^d Department of Geoscience, University of Wisconsin-Madison, 1215 W. Dayton Street, Madison, WI 53706, USA

^e Laboratoire des Sciences du Climat et de l'Environnement, UMR8212, IPSL-CEA-CNRS-UVSQ and Université Paris-Saclay, Domaine du CNRS Bât. 12, Avenue de la Terrasse, 91198 Gif-Sur-Yvette, France

^f Département de Préhistoire du Muséum national d'Histoire Naturelle, UMR 7194 du CNRS, 1 rue René Panhard, 75013 Paris, France

^g Ecole Française de Rome, Piazza Farnese 67, 00186 Roma, Italy

^h Sezione di Scienze preistoriche e antropologiche, Dipartimento di Studi Umanistici, Università degli Studi di Ferrara, C.so Ercole d'Este I, 32, Ferrara, Italy

ⁱ Berkeley Geochronology Center, 2455 Ridge Road, Berkeley, CA, 94709, USA

^j University of California, Department of Earth and Planetary Science, Berkeley, CA, 94720, USA

ARTICLE INFO

Article history:

Received 23 November 2015

Received in revised form 16 May 2016

Accepted 23 May 2016

Available online xxx

Editor: H. Stoll

Keywords:

aggradational succession

glacial termination

glacio-eustatic forcing

Tiber River

$^{40}\text{Ar}/^{39}\text{Ar}$ dating

ABSTRACT

We use 13 new $^{40}\text{Ar}/^{39}\text{Ar}$ and 4 new ^{14}C datings of volcanic deposits and organic material found within near-coastal aggradational successions deposited by the Tiber River near Rome, Italy, to integrate a larger dataset previously achieved in order to offer independent age constraints to the sea-level fluctuations associated with Late Quaternary glacial cycles during the last 450 ka. Results are compared with the chronologically independently constrained Red Sea relative sea-level curve, and with the astronomically tuned deep-sea benthic $\delta^{18}\text{O}$ record. We find good agreements for the timings of change, and in several cases for both the amplitudes and timings of change during glacial terminations T-1, T-2, T-3, and T-5. There is one striking exception, namely for glacial termination T-4 that led into interglacial Marine Isotope Stage (MIS) 9. T-4 in our results is dated a full 18 ka earlier than in the Red Sea and deep-sea benthic $\delta^{18}\text{O}$ records (which are in good agreement with each other in spite of their independent chronological constraints). The observed discrepancy is beyond the scale of the combined age uncertainties. One possible explanation is that the documented aggradation represents an early phase, triggered by a smaller event in the sea-level record, but the thickness of the aggradational sediment sequence then suggests that the amplitude of this earlier sea-level rise is underestimated in the Red Sea and benthic $\delta^{18}\text{O}$ records. Also, this would imply that the aggradational succession of the main T-4 deglaciation has not yet been located in the study region, which is hard to reconcile with our extensive fieldwork and borehole coverage, unless unlikely non-deposition or complete erosion. Resolving this discrepancy will improve understanding of the timing of deglaciations relative to the orbitally modulated insolation forcing of climate and will require further focused research, both into the nature and chronology of the Tiber sequences of this period, and into the chronologies of the Red Sea and deep-sea benthic $\delta^{18}\text{O}$ records.

© 2016 Elsevier B.V. All rights reserved.

1. Introduction

A general consensus on the pacing of the global climate system by orbital variations has been reached since the formulation of the Milankovitch's theory (1941), thanks to a number of stud-

ies that have demonstrated that the timing of glacial-interglacial cycles is tuned with the long-term variations of the incoming solar radiation caused by changes in the Earth's orbital geometry (e.g., Hays et al., 1976; Berger, 1978; Imbrie et al., 1984; Shackleton et al., 1984, 1990; Berger et al., 1994; Raymo et al., 2006; Huybers, 2006). However, the mechanisms that translate this forcing into regional and global climate changes continue to be de-

* Corresponding author.

E-mail address: fabrizio.marra@ingv.it (F. Marra).

Table 1¹⁴C ages.

Sample data	Measured radiocarbon age	$\delta^{13}\text{C}$	Conventional radiocarbon age (*)
Beta – 420362 SAMPLE: S2-C10-46.5 ANALYSIS: AMS-Standard delivery MATERIAL/PRETREATMENT: (wood): acid/alkali/acid 2 SIGMA CALIBRATION: Cal BC 9750–9720 (Cal BP 11700–11670) and Cal BC 9695–9380 (Cal BP 11645–11330)	10040 ± 30 BP	–26.5‰	10020 ± 30 BP
Beta – 420363 SAMPLE: S2-C11-49.5 ANALYSIS: AMS-Standard delivery MATERIAL/PRETREATMENT: (wood): acid/alkali/acid 2 SIGMA CALIBRATION: Cal BC 10095–9810 (Cal BP 12045–11760)	10240 ± 40 BP	–27.2‰	10200 ± 40 BP
Beta – 420364 SAMPLE: S3-C9-41.3 ANALYSIS: AMS-Standard delivery MATERIAL/PRETREATMENT: (wood): acid/alkali/acid 2 SIGMA CALIBRATION: Cal BC 7705–7695 (Cal BP 9655–9645) and Cal BC 7680–7590 (Cal BP 9630–9540)	8660 ± 30 BP	–26.3‰	8640 ± 30 BP
Beta – 420365 SAMPLE: S3-C12-55.5 ANALYSIS: AMS-Standard delivery MATERIAL/PRETREATMENT: (wood): acid/alkali/acid 2 SIGMA CALIBRATION: Cal BC 13195–12955 (Cal BP 15145–14905)	12660 ± 40 BP	–26.8‰	12630 ± 40 BP

Dates are reported as RCYBP (radiocarbon years before present, “present” = AD 1950). By international convention, the modern reference standard was 95% the ¹⁴C activity of the National Institute of Standards and Technology (NIST) Oxalic Acid (SRM 4990C) and calculated using the Libby ¹⁴C half-life (5568 years). Quoted errors represent 1 relative standard deviation statistics (68% probability) counting errors based on the combined measurements of the sample, background, and modern reference standards. Measured ¹³C/¹²C ratios ($\delta^{13}\text{C}$) were calculated relative to the PDB-1 standard.

The Conventional Radiocarbon Age represents the Measured Radiocarbon Age corrected for isotopic fractionation, calculated using the delta ¹³C. On rare occasion where the Conventional Radiocarbon Age was calculated using an assumed delta ¹³C, the ratio and the Conventional Radiocarbon Age will be followed by “*”. The Conventional Radiocarbon Age is not calendar calibrated. When available, the Calendar Calibrated result is calculated from the Conventional Radiocarbon Age and is listed as the “Two Sigma Calibrated Result” for each sample.

bated. The dramatic changes in continental ice volume and concomitant variation in global mean sea level represent perhaps the most salient climate response during glacial cycles and are together encoded in the changes in $\delta^{18}\text{O}$ of foraminifera in global sediments. However, independent chronological constraint on the $\delta^{18}\text{O}$ are largely lacking prior to 60 ka (the limit of ¹⁴C dating in marine sediments). The most widely used chronology for the benthic $\delta^{18}\text{O}$ record of glaciation relies on a stationary relationship with orbital forcing, in particular summer northern hemisphere insolation (Lisiecki and Raymo, 2005). The sea level component of planktic $\delta^{18}\text{O}$ variation is amplified in the Red Sea due to the shallow sill depth, and a chronology for this record has been estimated by assuming that the U/Th dated weak monsoon events in Asian speleothems can be correlated to dust flux events in the marine cores in which sea level history has been estimated (Grant et al., 2014). Despite these advances, a quantitative understanding of the relationship between ice volume and orbital forcing over the last 900 ka remains a challenge and several longstanding problems remain (Paillard, 2015, and references therein). Critically, it remains difficult to identify why the sudden melting of the ice sheets at glacial terminations occurs during certain maxima of summer Northern Hemisphere insolation but not all NH summer maxima (e.g.: Muller and MacDonald, 1997; Paillard, 1998), and more generally why the temperature and ice volume variations are asymmetrical despite more sinusoidal insolation forcing (Tziperman and Gildor, 2003). A major role for changes in the carbon cycle has been proposed to modulate the amplitude, and potentially the timing, of the glacial cycles over the last 900 ka but elucidating the orbital controls on the carbon cycle has been especially difficult (Paillard, 2015). Here, we focus on providing independent chronological control on these glacial terminations, in order to improve quantitative understanding of their relationship with orbital insolation changes.

We propose that independent chronological control of the glacial terminations can be attained by dating fluvial sediment

aggradation which is controlled by the rapid sea level rise during the glacial terminations. We study the aggradation sequences in the Tiber River in Italy, an ideal and unique setting because the frequent volcanic activity produces volcanic intercalations which can be independently dated using K–Ar. In the sections within 20 km of the modern coastline, the rise in base level during the rapid sea level rise causes aggradation and rapid deposition of a fining upward sequence. To date, the Tiber River aggradational successions represent the only geochronologically constrained, glacio-eustatically forced sedimentary record spanning MIS 1 through MIS 19, and therefore offers a unique opportunity to compare U/Th ages and astrochronological calibration of the global sea-level changes during glacial terminations. The potential of this record has been highlighted over the last decades, as ⁴⁰Ar/³⁹Ar dating of volcanic interbeds has provided independent chronology of the aggradations during glacial terminations (Alvarez et al., 1996; Karner and Renne, 1998; Karner and Marra, 1998; Marra et al., 1998; Karner et al., 2001a; Florindo et al., 2007). In the present paper we extend this record with four new ¹⁴C and thirteen new ⁴⁰Ar/³⁹Ar age determinations (Table 1 and 2), to provide the most complete geochronologic constraints on phases of sediment aggradation in the coast of Rome and to document the chronology of deglaciations relative to the orbitally modulated insolation forcing of climate.

2. Setting and methods

The Paleo Tiber River and its tributaries in the area of Rome have established a sensitive depositional response to sea level variations. To date ten aggradational sequences have been identified, corresponding to periods of rapid sea level rise since MIS 21, including the glacial terminations and several minor successions corresponding to the more pronounced $\delta^{18}\text{O}$ sub stages.

The sedimentary features of these aggradational successions encompass fluvial to lacustrine and lagoon to coastal facies (Conato

Table 2

Ar/Ar ages.

Sample	#Cryst	Lab	R-Acs	Age A		Age B		Age C		
				Age of Acs	Riv13	1.185	Nom05	1.194	Ren11	1.206
				Lambda	Min00	5.463E−10	SJ77	5.543E−10	Ren11	5.531E−10
				Age	±2σ	Age	±2σ	Age	±2σ	
NCR-2	6 of 9	WiscAr	0.108990457	129.2	1.5	130.2	1.5	131.4	1.5	
PdG-S13	1 of 12	WiscAr	0.207703849	246.2	3.9	248.1	3.9	250.5	3.9	
PdG-S22	3 of 12	WiscAr	0.220096156	260.9	5	262.9	5	265.4	5	
AV-AF	3 of 12	WiscAr	0.232657167	275.8	1.6	277.9	1.6	280.6	1.6	
PdG-S19	6 of 9	WiscAr	0.248927621	295.1	2.2	297.3	2.2	300.2	2.2	
CH-AF	9 of 12	WiscAr	0.294873614	349.5	1.7	352.2	1.7	355.6	1.7	
PdG-S23	5 of 5	BGC	0.221885908	263	8	265	8	268	8	
PdG-S4	5 of 5	BGC	0.226910117	269	6	271	6	274	6	
PdG-S2	6 of 6	BGC	0.366757312	435	10	438	10	442	10	
PdG-S12	2 of 5	BGC	0.375131806	445	10	448	10	452	10	
PdG-S6	4 of 5	BGC	0.38099398	452	18	455	18	459	18	
Tor 1 + POL12	3 of 10 + 5 of 15	Gif-sur-Yvette	0.2972508	452	4	355	4	358	4	

Sample	#Cryst	Lab	R-Acs	Age A		Age B		Age C		
				Age of Acs	Riv13	1.185	Nom05	1.194	Ren11	1.206
				Lambda	Min00	5.463E−10	SJ77	5.543E−10	Ren11	5.531E−10
				Age	±2σ	Age	±2σ	Age	±2σ	
From literature										
R93-15H2	4 of 6	BGC	0.211580912	251	8	253	8	255	8	
R95-04B*	5 of 6	BGC	0.224226121	266	5	268	5	270	5	
TGdSR93-28	6 of 6	BGC	0.23855749	283	2	285	2	288	2	
SPQR-51	7 of 7	BGC	0.348154741	413	11	416	11	420	11	
R95-04H**	3 of 6	BGC	0.365859654	434	8	437	8	441	8	
R94-30C	7 of 7	BGC	0.35574254	422	5	425	5	429	5	
Tufo Lionato	13 of 18	BGC	0.30562491	362	4	365	4	369	4	
C7	8 of 8	BGC	0.343308975	407	2	410	2	412	2	
POL 12-01/03	23 of 29	Gif-sur-Yvette	0.272128752	323	2	325	2	328	2	

Sample	#Cryst	Age A		Age B		Age C		
		Age of Acs	Riv13	1.185	Nom05	1.194	Ren11	1.206
		Lambda	Min00	5.463E−10	SJ77	5.543E−10	Ren11	5.531E−10
		Age	±2σ	Age	±2σ	Age	±2σ	
Combined ages								
PdG-S4+R95-04B	10 of 11	267.5	3.8	269.2	3.8	271.6	3.8	
PdG-S2+R95-04H	9 of 12	434.4	6.2	437.4	6.2	441.4	6.2	

Calibration references: Riv13 = [Rivera et al., 2013](#); Min00 = [Min et al., 2000](#); Nom05 = [Nomade et al., 2005](#); SJ77 = [Steiger and Jäger, 1977](#); Ren11 = [Renne et al., 2011](#).

[et al., 1980](#), and references therein). The lowering of sea level during each glacial period causes a coastline regression and base level drop, which produces a basal erosive surface and excavation. Subsequently, during the final stages of the lowstand at the onset of each glacial termination, coarse grained material is deposited. This is followed during the deglacial sea level rise by a rapidly deposited, fining upwards sequence, terminating in fine grained sediments which accumulate during the highstand. The thickness of this rapidly deposited sequence is proportional to accommodation space, giving indirect estimation of the amplitude of the full sea-level oscillation. Effect of the long term uplift, averaging 50 m over the past 500 hundred thousand years ([Karner et al., 2001a](#)), is negligible over the few ky duration of deposition of each aggradation sequence, whereas sudden tectonic collapse due to fault displacement may have larger influence and has to be evaluated carefully when relating the thickness of the sequence to the magnitude of sea level rise (e.g.: [Marra et al., 1998](#); [Florindo et al., 2007](#); [Marra and Florindo, 2014](#)).

Because of the basal erosion during lowstand, the stratigraphic record is discontinuous. The sediment packages deposited within the fluvial incisions and in the coastal plain have been designated by formal Formation names, newly conceived or based upon previous literature ([Karner and Marra, 1998](#), and references therein). A detailed facies analysis of the deposits cropping out in the coastal area of Rome describing a suite of fourth-order depositional

sequences was provided in [Milli \(1997\)](#), and partially revised later on [Milli et al. \(2008\)](#).

The most recent alluvial succession within the terminal tract of the Tiber's fluvial channel through the coastal plain has been extensively dated using the radiocarbon method ([Marra et al., 2008, 2013](#)). This revealed an abrupt transition from a basal 8–10 m thick coarse grained gravel layer, to an overlying 40–60 m thick sandy clay package, dated between narrow age bounds of 13.6 ± 0.2 and 12.8 ± 0.2 ka within the last deglaciation (glacial Termination 1, or T-1) ([Marra et al., 2008](#)). Accordingly, a conceptual model was proposed, in which gravel-clay transitions serve as a proxy for glacial terminations. Application of the conceptual model to older successions revealed good general agreement between the tephra-based $^{40}\text{Ar}/^{39}\text{Ar}$ ages for glacial terminations and the astronomically tuned chronology of deep-sea benthic $\delta^{18}\text{O}$ records, with a few possible misfits (for T-4 and T-7), as discussed in [Marra et al. \(2008\)](#) and [Marra and Florindo \(2014\)](#).

Here, we first strengthen the temporal constraints on the sedimentary transition in the most recent aggradational succession with four additional ^{14}C age dates, based on wood samples collected at different elevations throughout the basal gravel layer in a borehole from the Tiber Valley in Rome. We demonstrate a close timing agreement between the gravel-clay transition, which is recognized throughout a 20 km-long tract of the Tiber channel and in the modern coastal plain, and the interval of fastest sea-level rise within T-1 ([Stanford et al., 2011](#)).

Next, we provide 13 new $^{40}\text{Ar}/^{39}\text{Ar}$ dates on as many tephra layers found within older aggradational successions of the Paleo-Tiber River. These new dates reinforce the concept that these aggradational sequences correspond to phases of sea-level rise during the deglaciations into Marine Isotopic Stages (MIS) 5, 7, 9, and 11 (i.e., T-2, T-3, T-4, and T-5, respectively). Combining our new dates with previous dates, we obtain strong independent age control for T-2, T-3, T-4, and T-5. In addition, we gain new insights into the durations of these sea-level rises, which complement information obtained from other, independent sea-level records (e.g. Grant et al., 2012; 2014).

2.1. ^{14}C analyses

Radiocarbon dating analyses were performed at Beta Analytic Inc. Laboratory, Miami, Florida, accredited to ISO/IEC 17025:2005 Testing Accreditation PjLA #59423 standards. Methods are reported in Table 1 along with results. The Conventional Radiocarbon Ages have all been corrected for total fractionation effects and where applicable, calibration was performed using 2013 calibration databases (see Supplementary online material #2).

2.2. $^{40}\text{Ar}/^{39}\text{Ar}$ analysis

The $^{40}\text{Ar}/^{39}\text{Ar}$ ages used in this paper to constrain aggradation of the sedimentary successions of the Paleo-Tiber River have been performed over the last two decades in different laboratories (Appendixes A, B and C3), which have used different standards and different calibrations for the ages of these standards (Renne et al., 1998, 2011; Kuiper et al., 2008). In particular, the $^{40}\text{Ar}/^{39}\text{Ar}$ dates presented here are calculated relative to the Alder Creek rhyolite sanidine standard (ACs), which has proposed ages ranging from 1.185 to 1.206 Ma (Rivera et al., 2013; Nomade et al., 2005; Renne et al., 2011) (Table 2). To ease comparison with published $^{40}\text{Ar}/^{39}\text{Ar}$ ages for the aggradational successions of the Paleo-Tiber (Marra et al., 2008; Marra and Florindo, 2014) we discuss all new $^{40}\text{Ar}/^{39}\text{Ar}$ ages herein relative to an ACs age of 1.194 Ma (Nomade et al., 2005), without necessarily endorsing these values. Considering the fact that our $^{40}\text{Ar}/^{39}\text{Ar}$ ages have uncertainties ranging between 2 and 8 ky (see Table 2), and that the uncertainties associated with the astronomical tuning of the $\delta^{18}\text{O}$ record (Lisiecki and Raymo, 2005) and the U/Th-derived chronology of the Red Sea sea-level record (Grant et al., 2014) that we compare with are of the same order, the choice of $^{40}\text{Ar}/^{39}\text{Ar}$ standard age calibration is essentially negligible in the discussion of the timing of glacial terminations.

2.2.1. $^{40}\text{Ar}/^{39}\text{Ar}$ protocol WiscAr

Age determination was performed at the University of Wisconsin Rare Gas Geochronology Laboratory by single crystal total fusion on sanidine from pyroclastic-flow samples. Sample preparation and analytical procedures follow those in Jicha et al. (2012). Full data are found in Appendix A.

2.2.2. $^{40}\text{Ar}/^{39}\text{Ar}$ protocol BGC

Facilities and methods used at BGC were substantially as reported by Karner and Renne (1998) except that a CO_2 laser was used for sample fusions and Alder Creek sanidine (ACs; Nomade et al., 2005) was used as a neutron fluence monitor for all samples. Statistical data in Appendix B.

2.2.3. $^{40}\text{Ar}/^{39}\text{Ar}$ protocol Gif-sur-Yvette

After crushing and sieving of volcanic deposits extracted from each unit, pristine sanidine crystals ranging from 500 μm up to 1 mm in size are extracted. Crystals are handpicked under a binocular microscope and slightly leached for 5 min in a 7 % HF acid

solution in order to remove groundmass that might still be attached to them. After leaching, at least 30 crystals are handpicked for each sample and separately loaded in aluminum disks. The samples are then irradiated for 1 h (IRR 85 and 77) in the $\beta 1$ tube of the OSIRIS reactor (CEA Saclay, France). After irradiation between 10 and 15 crystals for each unit are loaded individually in a copper sample holder. The sample holder is then put into a double vacuum Cleartran window. Each sanidine is fused using a Synrad CO_2 laser at 10 to 15% of nominal power (ca. 75 Watts). The extracted gas is then purified for 10 min by two hot GP 110 getters (ZrAl). Argon's isotopes (^{36}Ar , ^{37}Ar , ^{38}Ar , ^{39}Ar and ^{40}Ar) are analyzed using a VG5400 mass spectrometer equipped with an electron multiplier Balzers 217 SEV SEN coupled to an ion counter. We follow the full analytical protocol outlined in detail in Nomade et al. (2005). Neutron fluence J for each sample is calculated using co-irradiated Alder Creek Sanidine (AC) standard with an age of 1.194 Ma (Nomade et al., 2005) and the total decay constant of Steiger and Jäger's (1977). Recent revisions of the standard and/or decay constants suggest values of about $\pm 1\%$ greater than the one we used. Nevertheless, the difference in the final age for levels dated is negligible well within the full-propagated uncertainties (Kuiper et al., 2008; Renne et al., 2011; Phillips and Matchan, 2013; Rivera et al., 2013). Procedural blank measurements are computed after every three unknown samples. For typical 9 min static blank, typical backgrounds are about $2.0\text{--}3.0 \times 10^{-17}$ and 5.0 to 6.0×10^{-19} moles for ^{40}Ar and ^{36}Ar respectively. The precision and accuracy of the mass discrimination correction was monitored by weekly measurements of air argon of various beam sizes. Full data in Appendix C.

3. Results and discussion

3.1. Termination I and MIS 1

In Fig. 1a, we show our ^{14}C constraints on sediment aggradation within the Tiber River Valley since the Last Glacial maximum. An overall synchronous aggradation of clastic sediments characterizes the >20 km terminal tract of the fluvial channel and the coastal plain (Fig. 1b), as evidenced by a sharp lithological transition between gravel and clay that formed between 13.6 ± 0.2 and 12.8 ± 0.2 cal BP ka, and by parallel, sub-horizontal isochron lines across the upper package of clayey sediments (Fig. 1a). The new geochronologic constraints provided here for the basal portion of the gravel bed (MAXXI borehole, suppl. material #1; D in cross-section of Fig. 1a) show that most of the gravel aggradation occurred since 15 ka, as evidenced by a cal BP age of 15.025 ± 0.12 ka for a sample collected 0.7 m above the base of the gravel layer (Table 1).

The timing of the sedimentary switch to fine sediments overlaps the youngest portion of the time-window of meltwater pulse (mwp) 1a, as statistically identified in Stanford et al. (2011), closely following the maximum rate of sea-level rise of this event. Gravel deposition broadly coincided with the Bølling warming and early to peak phases of mwp-1a (Fig. 1c).

Consistent with these observations, Marra et al. (2013) proposed that transportation of very coarse gravel (>5 cm diameter) by the Tiber River requires exceptional hydrologic conditions that were seen during terminations only, and that have not been repeated during the Holocene. Such conditions existed due to a combination of: (i) increased sediment supply to the Tiber drainage basin due to rapid melting of Apennine glaciers that released large amounts of clastic material; and (ii) low sea levels that caused a steep topographic gradient, hence greater and more energetic river transport capacity. Eventually, accelerated sea-level rise during terminations caused a rapid drop in transport capacity of the Tiber River, which in turn resulted in sandy clay deposition in a less

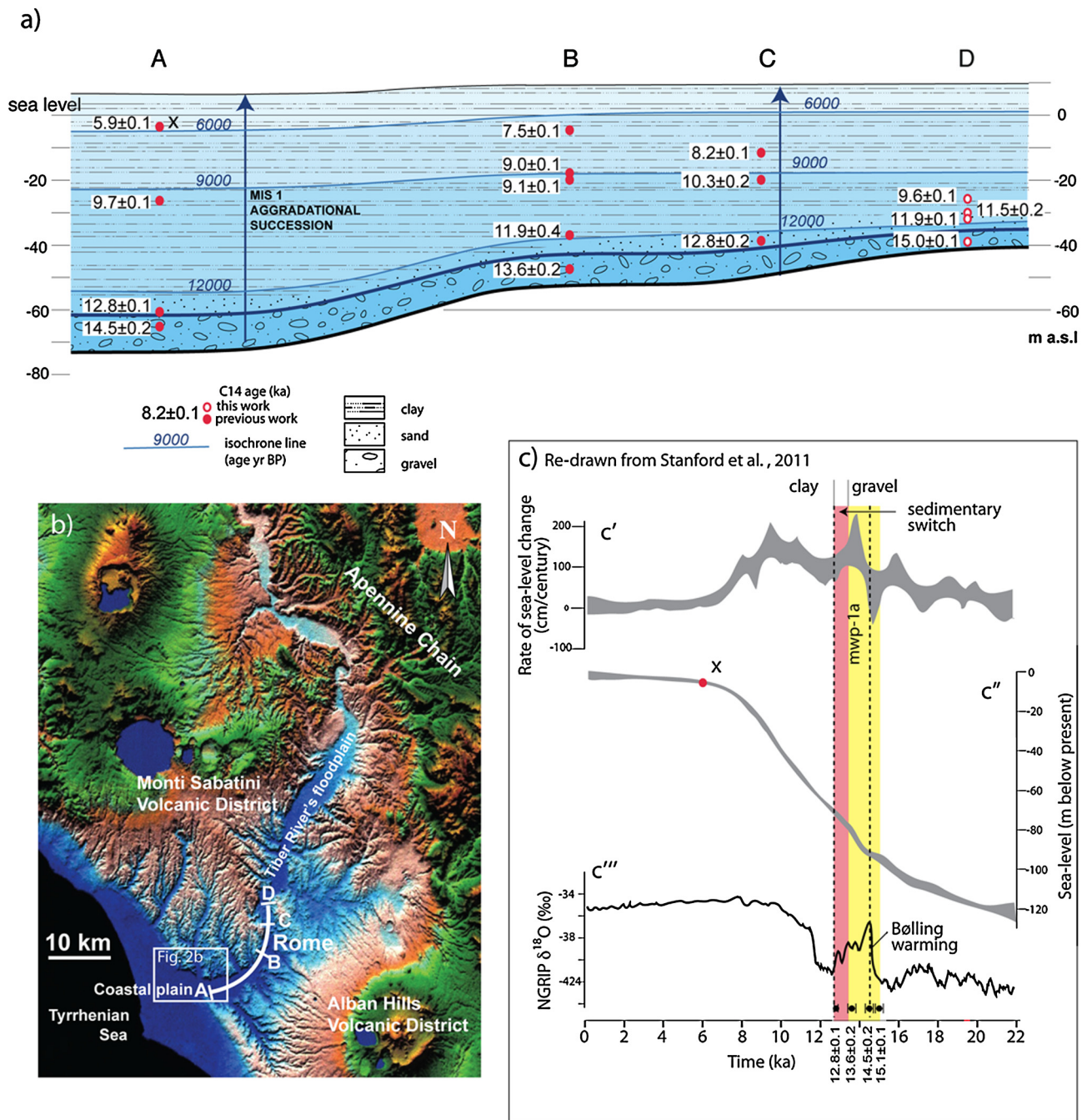


Fig. 1. a) Longitudinal cross-section showing the geochronologic constraints to sediment aggradation within the modern Tiber River fluvial incision near the coast. b) Investigated area and location of cross-section. Most of the gravel deposition occurred between 15.0 ± 0.1 and 13.6 ± 0.2 ka, while the abrupt sedimentary switch from a basal coarse gravel bed to an overlying clay section occurs synchronously along the 20 km-long investigated tract of the valley, bracketed by the ^{14}C ages of 13.6 ± 0.2 and 12.8 ± 0.2 ka. c) The age interval of gravel deposition (yellow vertical bar) and of the sedimentary shift (red vertical bar) is compared with a statistically assessed (95% confidence) rate of sea-level change (c') and global sea-level curve (c''), and with the NGRIP $\delta^{18}\text{O}$ record (c''') (Stanford et al., 2011, and references therein), evidencing that gravel deposition is broadly coincident with the Bølling warming event, and that the sedimentary switch overlaps the youngest portion of the time-window of meltwater pulse (mwp) 1a, closely following the maximum rate of sea-level rise of this event. (For interpretation of the references to color in this figure legend, the reader is referred to the web version of this article.)

energetic environment. Finally, almost complete infilling occurred of the fluvial incision that was excavated during the lowstand. Thus, the floodplain approached present-day sea level, which for the last glacial termination occurred at around 6000 yr BP (level X in Figs. 1a and 1c).

Following this conceptual framework, we apply the coincidence of the gravel-to-clay transition with a key phase of fast (deglacial) sea-level rise, to obtain ages for previous deglacial sea-level rises. In particular, we use the method to assess the ages of glacial ter-

minations T-2 to T-5, by providing $^{40}\text{Ar}/^{39}\text{Ar}$ ages at, or close to, the gravel-clay transition in the older aggradational successions of the Paleo-Tiber River. To do so, we combine 12 new and 11 previous $^{40}\text{Ar}/^{39}\text{Ar}$ ages (with uncertainties reported at 2σ) to date the glacial terminations in the Tiber sequence. We compare these independent, radioisotopic ages with the recent sea-level chronology of Grant et al. (2012, 2014), which was indirectly constrained by U/Th ages.

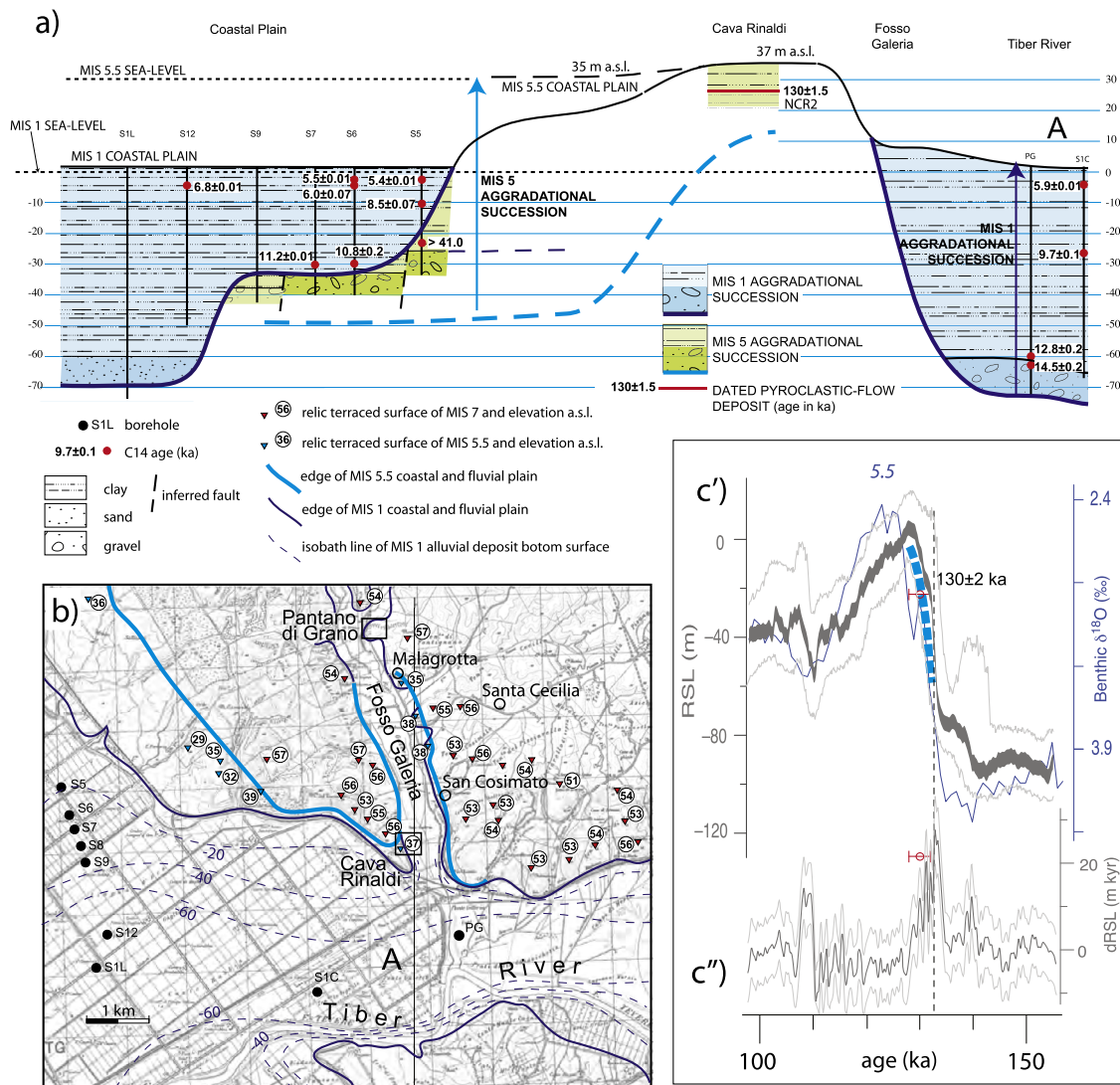


Fig. 2. a) Composite cross-section showing the geochronologic constraints to the last two aggradational successions (MIS 5.5 and MIS 1) deposited in the terminal tract of the Tiber Valley and in the inner coastal area of Rome (b), reconstructed after borehole and ^{14}C data from Belluomini et al. (1986); Bellotti et al. (2007); Marra et al. (2013), and after $^{40}Ar/^{39}Ar$ age and field data from Marra et al. (2015). c) Aggradation of the fine grained portion of MIS 5.5 succession, constrained by an age of 130 ± 2 ka for the dated pyroclastic layer (dashed blue line), is compared to the curves of relative sea-level (RSL) and rate of change in sea-level (dRSL) by Grant et al. (2014) (thinner lines: 95% confidence intervals), and with the deep-sea benthic $\delta^{18}O$ record by Lisiecki and Raymo (2005). This sedimentary event occurs shortly after the glacial termination (dotted vertical line in c'), consistent with assumption that the deposition of the basal gravel is triggered by the maximum rate of sea-level rise during the glacial termination (c'). (For interpretation of the references to color in this figure legend, the reader is referred to the web version of this article.)

3.2. Glacial termination II and MIS 5.5

A composite cross-section (Fig. 2a) shows the stratigraphic setting of the terminal tract of the Tiber River's fluvial valley and the inland portion of the coastal plain (Fig. 2b, see also map in Fig. 1b). Borehole and radiocarbon data constrain the part of the sequence that formed in response to sea-level rise during the last deglaciation in this sector (Belluomini et al., 1986; Bellotti et al., 2007; Marra et al., 2013), while geometry and stratigraphy of a preceding aggradational cycle were reconstructed in Marra et al. (2015). This integrates a new geochronological datum from Cava Rinaldi with geomorphologic investigation and previous borehole data. A $^{40}Ar/^{39}Ar$ age of 130 ± 1.5 ka (Table 2) was found for a pyroclastic-flow deposit intercalated within a fluvial-lacustrine deposit at Cava Rinaldi, near the confluence of the Fosso Galeria stream valley with the Tiber River alluvial plain (Fig. 1a and 1b). This confirmed that the pre-MIS 1 sedimentary cycle corresponds to the deglacial sea-level rise of T-2 that led into MIS 5.5 (the last interglacial) (Marra et al., 2015). The coastal terrace of this

aggradational succession resides at 36–39 m a.s.l. (blue triangles in Fig. 2b). Our results revise previous partial attribution of this paleo-surface to MIS 7 (Sorgi, 1994; Karner et al., 2001a). Instead, we identify the widespread paleo-surface with a top at 53–57 m a.s.l. (Karner et al., 2001) (red triangles in Fig. 2b) as the coastal plain terrace of MIS 7. That MIS 7 terrace therefore seems to have been uplifted by about 65 m since 200 ka, assuming an original sea-level position of roughly -10 m, relative to the present day (Rohling et al., 2009).

Both the stratigraphic position relative to the basal gravel layer, and the absolute elevation (26 m a.s.l.) of the 130 ± 1.5 ka pyroclastic-flow deposit appear to be indicative of the final stages of the fastest portion of the T-2 sea-level rise, similar to our observations for T-1 (Fig. 2a, c). The thickness of the MIS 5 aggradational succession between the base level and the dated pyroclastic layer is ~ 65 m, which is remarkably consistent with a sea-level jump of about 60 m between 135 and 130 ka, which was associated with an interval commonly identified as Heinrich Event 11 (Grant et al., 2012, 2014; Marino et al., 2015) (Fig. 2c).

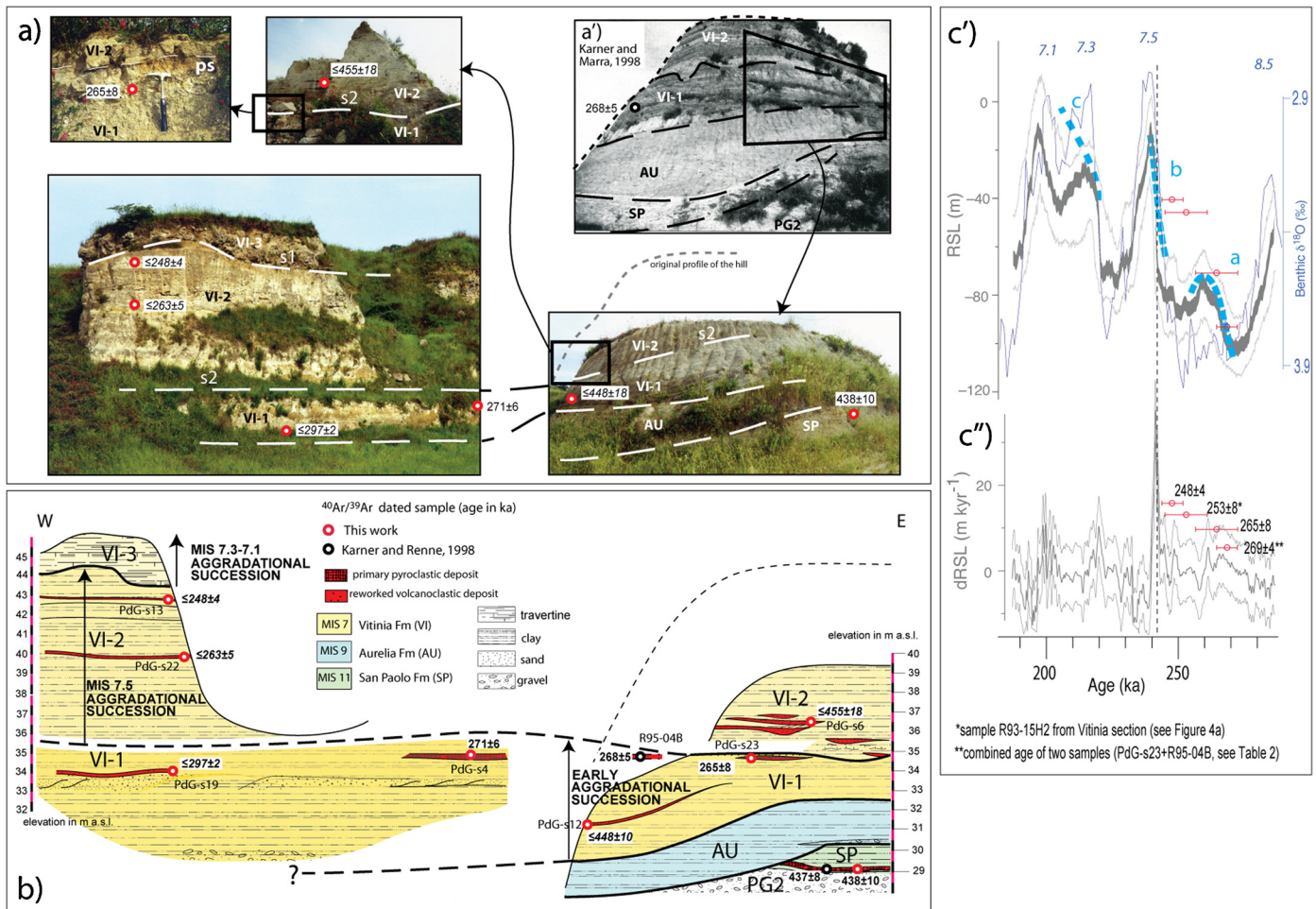


Fig. 3. a) Photographs showing general stratigraphy and some detail (see section 3.3) of the Pantano di Grano outcrops investigated in the present work. The setting at the time of the previous investigation by [Karner and Marra \(1998\)](#) is also shown (a'). b) Geologic cross-section showing the aggradational succession of the Vitinia Formation and the location of the volcanoclastic layers sampled for $^{40}\text{Ar}/^{39}\text{Ar}$ dating. Ages of reworked volcanic layers, in italics, are preceded by \leq to imply that the age of the sediment is equal or younger than the age provided by the sample. c) Our age of 248 ± 4 ka is assumed to be a close *post-quem* for glacial termination T-3 (see text for explanation) and is compared with the curves of relative sea-level (RSL) and rate of change in sea-level (dRSL) by [Grant et al. \(2014\)](#) (thinner lines: 95% confidence intervals), and with the deep-sea benthic $\delta^{18}\text{O}$ record by [Lisiecki and Raymo \(2005\)](#). (For interpretation of the references to color in this figure, the reader is referred to the web version of this article.)

3.3. Glacial termination III and MIS 7

A complex stratigraphic and aggradational pattern characterizes the sedimentary deposits of the Vitinia Formation at the Pantano di Grano locality ([Karner and Marra, 1998](#)). Here, we present results from a new field survey conducted at this site (the newly investigated sections are shown in the pictures of [Fig. 3a](#)), after the original outcrop (b&w picture from [Karner and Marra, 1998](#) in [Fig. 3a'](#)) was partially disrupted to enlarge the Malagrotta refuse disposal site.

The two pictures in the lower part of [Fig. 3a](#) display the remnant of the outcrop sampled by [Karner and Marra \(1998\)](#) (to the right = east), with the position of the new samples collected and dated for the present study ($^{40}\text{Ar}/^{39}\text{Ar}$ ages in ka are reported), and the newly sampled section (to the left = west), which is located 100 m northeast of the previous outcrop. Details of the upper portion of the first outcrop are shown in the two pictures in the left upper part of [Fig. 3a](#), reporting position and ages of two other samples dated here, and location of a paleosol (ps) detected during the new field survey. Lithostratigraphy of the two outcrops with position of all the sampled volcanic layers is also reported in the schemes of [Fig. 3b](#), showing that well-bedded, white sandy-clayey deposits with freshwater gastropods (*Bithynia tentaculata*, the common faucet snail) and brackish-to-saltwater mollusks (*Cerastoderma edule*, the common cockle) alternate with diatoma-

ceous layers in the central portion of this succession. There are several intercalations of fine-grained gravels that contain abundant reworked volcanoclastic material. A medium-sized, mostly sedimentary gravel layer occupies the lowest portion of the section at the western outcrop ([Fig. 3b](#)). However, its base is not exposed, which prevents us from estimating the total thickness of the aggradational succession. The upper part of the succession is truncated by an unconformable contact (s1 in [Fig. 3a](#)), above which travertine deposits occur. Our new field survey also revealed another, previously undetected, sedimentary hiatus (s2), based on a paleosol (ps) in the lower portion of the eastern outcrop (see detail pictures in [Fig. 3a](#)). The paleosol is not exposed in the western outcrop, likely due to the vegetation cover ([Fig. 3a](#)).

Seven samples were collected for $^{40}\text{Ar}/^{39}\text{Ar}$ date from volcanoclastic layers within the Vitinia Formation succession at Pantano di Grano. These samples were dated in two distinct experiments conducted at the Berkeley Geochronology Center (PdG-s4, PdG-s6, PdG-s12, PdG-s23, [Table 2](#)) and at the WiscAr Laboratory at the University of Wisconsin-Madison (PdG-s13, PdG-s19, PdG-s22, [Table 2](#)). Only one of these samples (PdG-s4) was collected from a layer with evident features of a primary pyroclastic-flow deposit, while the remaining ones should be considered as providing *post-quem* ages (i.e., an oldest possible age for the sediment in which the volcanic material is re-deposited).

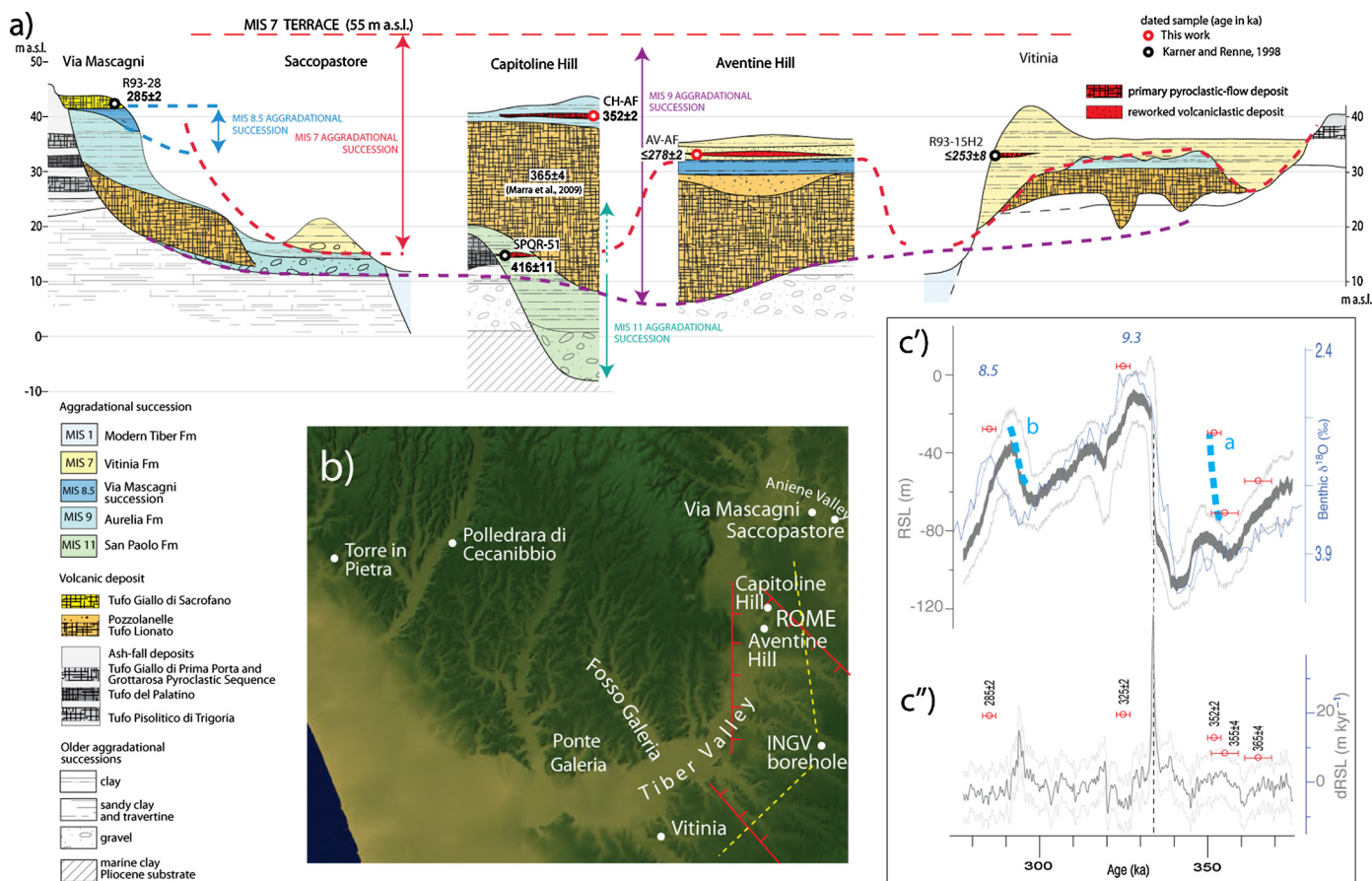


Fig. 4. a) Composite cross-section showing the stratigraphic correlation and the geochronologic constraints of the Aurelia Formation (MIS 9) relative to other aggradational successions cropping out in the investigated area (b). c) An age of 352 ± 2 ka, based on the dated sample from Capitoline Hill, constrains aggradation of the fine-grained portion of the sedimentary succession (dashed blue line a), which considerably pre-dates glacial termination T-4 in the Grant et al. (2014) reconstruction and in the deep-sea benthic $\delta^{18}\text{O}$ record by Lisiecki and Raymo (2005), while it appears coincident with an early, minor peak of sea level rise (see text for discussion). In contrast, an age of 285 ± 2 ka for the Tufo Giallo di Sacrofano provides a good match between aggradation of the Via Mascagni succession (dashed blue line b) and the sea-level reconstruction of Grant et al. (2014), and accounts for correlation with marine isotopic sub-stage 8.5. (For interpretation of the references to color in this figure legend, the reader is referred to the web version of this article.)

Based on stratigraphic position, primary depositional features, and indistinguishable radiometric ages, the volcanic deposit sampled at the western section (PdG-s4) and that previously sampled at the eastern outcrop (R95-04B) are considered to be the same, dated here at 271 ± 6 ka, and dated previously at 268 ± 5 ka (Karner and Renne, 1998), respectively. We have therefore recalculated a combined age of 269 ± 4 ka for this deposit, from the weighted mean age of the two crystal populations (Table 2). This pyroclastic deposit is no longer present at the eastern section, due to removal of a large portion of the original outcrop. Regardless, the age of 265 ± 8 ka from a homogeneous population of five crystals collected within the paleosol at this outcrop (sample PdG-s23) provides a further, upper constraint to aggradation of the lower succession of the Vitinia Formation (VI-1), which contains the pyroclastic flow-deposit of PdG-s4 and R95-04B. In summary, we have a first unit of aggradation that dates to about 269 ± 4 ka, followed by stasis around 257 ka as evidenced by the paleosol, and a new phase of aggradation shortly after 248 ± 4 ka (PdG-s13). The latter is corroborated by a previous age of 252 ± 8 ka (Karner and Renne, 1998) from a pyroclastic layer at a similar stratigraphic level in another aggradational section of the Vitinia Formation (Fig. 4a), at its type-locality in southern Rome (Karner and Marra, 1998). Similar to PdG-s13, however, this previously dated sample contains a scattered age-population of crystals with a youngest one at 253 ± 8 ka, suggesting that it did not come from a primary deposit, but from a reworked deposit. Accordingly, also the age of

253 ± 8 ka should also be considered a *post-quem* for aggradation of the second VI-2 fine-grained section.

Our inferred early aggradation phase at around 269 ± 4 ka does not match the timing of the main sea-level rise in T-3 in the sea-level curve of Grant et al. (2014). Instead, this aggradation event seems to match a smaller and earlier sea-level rise in that reconstruction (dashed blue line a in Fig. 3c'). Roughly around 265 ± 8 ka (PdG-s23, collected in the paleosol at the top of the VI-1 succession), this early sea-level rise ended and gave way to a sea-level fall that caused sub-areal exposure of the lacustrine deposit of the Vitinia Formation at Pantano di Grano. This led to formation of a sedimentary hiatus (s2) that is represented by the paleosol.

If viewed in terms of accommodation space, the stratigraphic thicknesses of ca. 6 m deposited over a timescale of only a few thousand years suggests that the sea-level rise associated with aggradation of unit VI-1 was relatively small, compared to an overall thickness of up to 40 m for the complete suite of deposits in the Vitinia Formation near Rome, from a base level at 15 m a.s.l. to a top surface at 55–57 m a.s.l. in Saccopastore (Fig. 4a) (Marra et al., 2015).

The age of 248 ± 4 ka of PdG-s13 for the second aggradation sequence (VI-2) is slightly (ca. 2 ka) older than the dRSL peak in Grant et al.'s (2014) reconstruction (Fig. 3c''), in agreement with the reworked feature of the dated pyroclastic deposits. If we assume that the actual aggradation of VI-2 happened shortly after

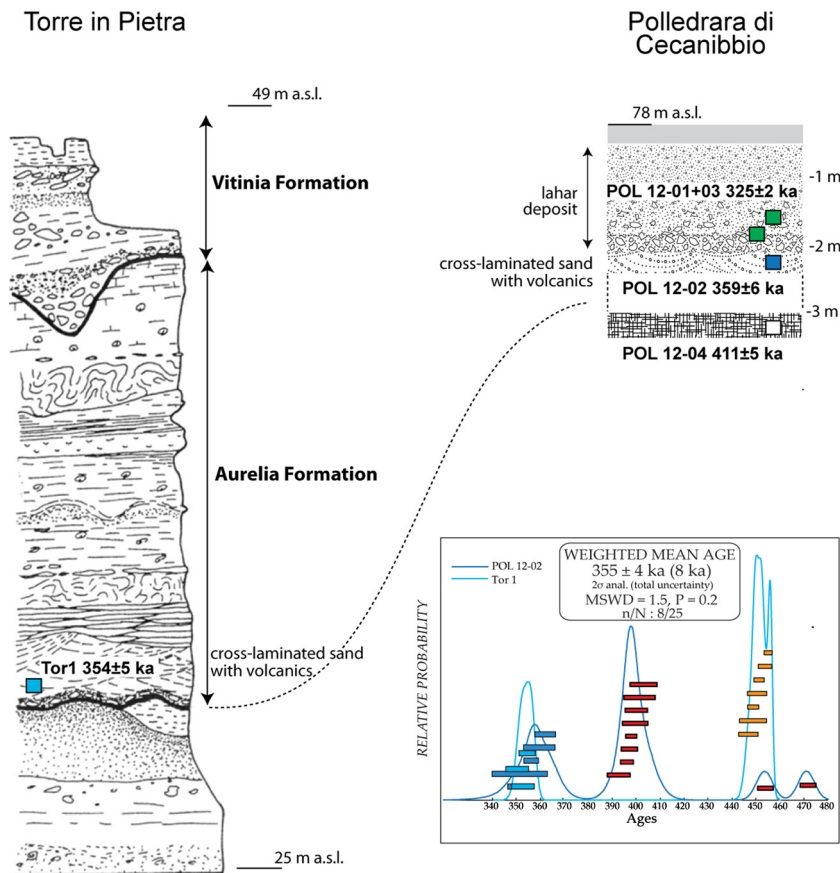


Fig. 5. a) Stratigraphy and geochronologic constraints of the Torre in Pietra (Grimaldi, 1998) and Polledrara di Cecanibbio (Anzidei et al., 2012) geologic sections. See section 3.4 for comments. b) Statistic diagram showing age distribution and weighted mean for samples Tor 1 and POL 12-02.

that age (as would be the case with reworking of fresh material), then the result gives a good match with the peak of sea-level rise (dashed blue line b in Fig. 3c').

Unit VI-2 is followed by unconformity surface s1, which in turn is followed by a third aggradational succession (VI-3 in Fig. 3). The elevation of 44 m a.s.l. for unit VI-3 rules out correlation with MIS 5.5, whose aggradational succession has top surface around 38 m a.s.l. in this area (Fig. 2b) (Marra et al., 2015). We therefore infer that VI-3 may represent a third phase of sea-level rise within MIS 7 (labeled c in Fig. 3c'). As yet, we do not have any dates to corroborate this suggestion, which therefore relies on stratigraphic context only.

3.4. Glacial termination IV and MIS 9

Deposition of the Aurelia Formation (Fig. 4) has been attributed to T-4 (Karner and Marra, 1998). This aggradational succession is bracketed by the Tufo Lionato and Tufo Giallo di Sacrofano pyroclastic-flow deposits, dated at 365 ± 4 ka (Marra et al., 2009) and 285 ± 2 ka (Karner et al., 2001b), respectively (Fig. 4a). Note that this interval also encompasses a minor aggradational succession that unconformably overlies the Aurelia Formation, and which may represent a sea-level rise associated with Marine Isotope Substage 8.5 (Fig. 4a, c; Marra et al., 2014).

We add a new date for a primary pyroclastic-flow deposit that is intercalated within fluvio-lacustrine deposits overlying the Tufo Lionato on the top of the Capitoline Hill. With an age of 352 ± 2 ka (Fig. 4a), this yields the first direct geochronologic constraint to aggradation of the Aurelia Formation. This dated sample (CH-AF) comes from a stratigraphic position at ~35 m above the base of the Aurelia Formation (Fig. 4a), where the latter is represented by

the gravel layer and/or the base of the Tufo Lionato pyroclastic-flow deposit of 365 ± 4 ka. Given this stratigraphic position, emplacement of the CH-AF pyroclastic layer (352 ± 2 ka) should be considered to postdate the sea-level rise of T-4. However, this age instead considerably pre-dates (>10 ka) the main sea-level rise of T-4 in the Grant et al. (2014) reconstruction (Fig. 4c), while the latter agrees with the astronomically tuned age for T-4 in the deep-sea benthic $\delta^{18}\text{O}$ record (Lisiecki and Raymo, 2005).

In contrast to our age of sample CH-AF (352 ± 2 ka), an age of 325 ± 2 ka was recently reported for another sample from deposits with a Middle Pleistocene faunal assemblage in the archaeological site of Polledrara di Cecanibbio (POL; see Fig. 4b for location) (Nomade et al., 2014, Table 2). This fauna is attributed to the Aurelian Mammal Age and to the Aurelia Formation (Anzidei et al., 2012). However, the sample from POL originates from a lahar deposit emplaced above fluvial sediments (Fig. 5), so that its age does not link directly to the fluvio-lacustrine succession that was deposited in response to sea-level rise during T-4. Instead, it offers an *ante-quem* (i.e., a youngest possible age for the sediment in which the volcanic material is re-deposited) age for T-4 (Fig. 4c). A second sample, which was collected in the fluvial sand underlying the lahar deposit (Fig. 5), contained a heterogeneous population of crystals with a youngest value of 359 ± 6 ka (Alison Pereira PhD thesis, pers. com.). This age is consistent with that for a re-worked volcanoclastic layer at the base of the Aurelia Formation at the Torre in Pietra (TIP) archaeological section; (Grimaldi, 1998, and references therein), which has a date as young as 354 ± 5 ka (Alison Pereira PhD thesis, pers. com.; Table 2, Fig. 5). Although re-worked, the lack of any crystals younger than 354 ± 5 ka in the medium-sized, lower portion of the aggradational sections of the Aurelia Formation at POL and TIP suggests a likely aggradation at

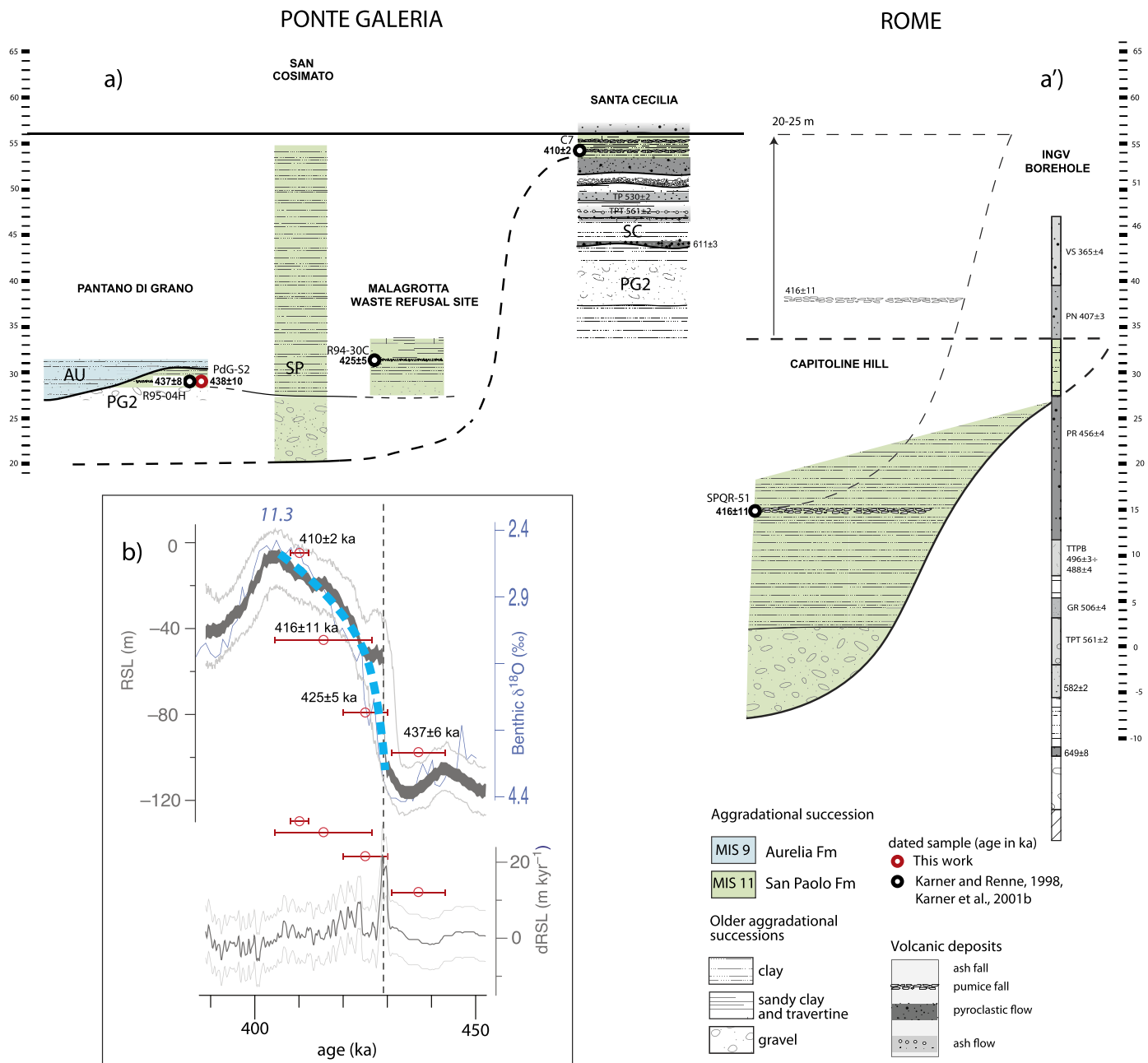


Fig. 6. a) Composite cross-section (see location in Fig. 4b) showing stratigraphic correlation and geochronologic constraints for different sedimentary successions of the San Paolo Formation (Karner and Marra, 1998). a') Geochronologic constraint (Karner and Marra, 1998) and geometry of the San Paolo formation outcrop at the Capitoline Hill (Corazza et al., 2004), correlated with the equivalent sedimentary deposit of MIS 11 recovered at the ING V borehole (See Fig. 4b for location), providing evidence of significant tectonic displacement of the Rome area with respect to Ponte Galeria. According to palynostratigraphic reconstruction in Marra and Florindo (2014), a ca. 20 m fault displacement restores the original elevation (dashed boundary of the aggradational succession). b) Ages of volcanic layers intercalated at different stratigraphic levels within the sedimentary successions, spanning 425 ± 5 to 410 ± 2 ka, constrain aggradation of the fine-grained portion (dashed blue line) in good agreement with the occurrence of glacial termination T-4 in the Grant et al. (2014) sea-level curve, and with the long duration of MIS 11 (Lisiecki and Raymo, 2005). In contrast, an age of 437 ± 6 ka (combined age of two samples) for the tephra above the basal gravel layer of the San Paolo Formation at Pantano di Grano significantly pre-dates this glacio-eustatic event, suggesting the occurrence of an early phase of aggradation during the minor peak of sea-level depicted in Grant et al.'s (2014) reconstruction. (For interpretation of the references to color in this figure legend, the reader is referred to the web version of this article.)

around 350 ka, in agreement with our new results for sample CH-AF (352 ± 2 ka).

An inferred thickness of 30 to 35 m (Fig. 4a) for the Aurelia Formation at Capitoline Hill suggests that its aggradation was driven by a large-amplitude sea-level rise (dashed blue line a in Fig. 4c). That, in turn, suggests a distinct mismatch with the chronology of the sea-level reconstruction of Grant et al. (2014), as well as with the astronomically tuned age for T-4 in deep-sea benthic $\delta^{18}O$ records (Lisiecki and Raymo, 2005). The age of 352 ± 2 ka for sample CH-AF may imply that the observed Aurelia Formation instead

corresponds to an early ~ 20 m sea-level rise in the Red Sea reconstruction at exactly that age (Fig. 4c); if true, then the aggradation phase related to the main deglaciation into MIS 9 has not been found yet.

In contrast to the complication with T-4, our age of 285 ± 2 ka for the Tufo Giallo di Sacrofano (left-hand side of Fig. 4a) offers a good match between the aggradation that we attribute to sea-level rise associated with Marine Isotope Sub-stage 8.5, and the sea-level reconstruction of Grant et al. (2014) (dashed blue line b in Fig. 4c). The Tufo Giallo di Sacrofano caps the sedimentation

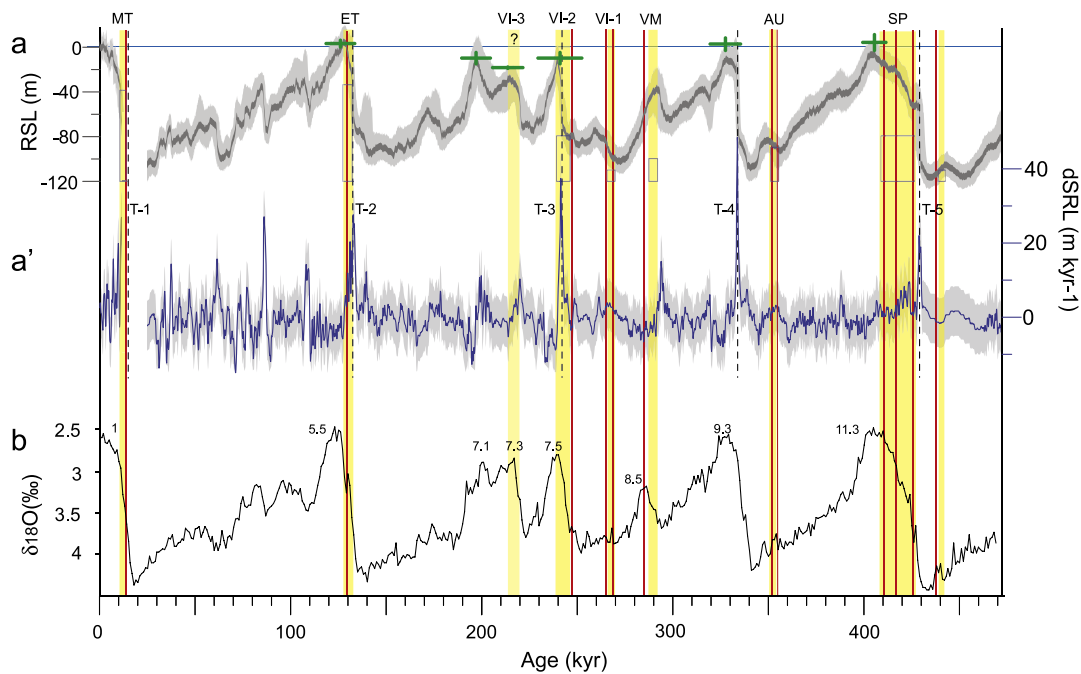


Fig. 7. Phases of aggradation in the coastal area of Rome (yellow vertical bars; vertical height of the boxes represents the observed thickness of the aggradational successions), as provided by the geochronologically constrained aggradational successions of the Paleo-Tiber River, compared with the independently dated curves of relative sea-level and rate of sea-level change (Grant et al., 2014) (gray shade: 95% confidence intervals), and with the astronomically tuned deep-sea benthic $\delta^{18}\text{O}$ curve (Lisiecki and Raymo, 2005). Red vertical lines correspond to mean weighted ages of intercalated pyroclastic layers. Dotted black lines are the glacial terminations T-2 through T-5 corresponding to maximum rates of sea-level rise in the dRSL curve. The green symbols in the first row are coral and speleothem-based sea-level markers (Rohling et al., 2009). MT: Modern Tiber Formation; ET: Epi-Tyrrhenian Formation; VI: Vitinia Formation; AU: Aurelia Formation; VM: Via Mascagni succession; SP: San Paolo Formation. (For interpretation of the references to color in this figure legend, the reader is referred to the web version of this article.)

of the aggradational Via Mascagni sub-sequence (Fig. 4a), and accordingly closely post-dates the sharp sea-level rise at 293 ka in the Grant et al. (2014) reconstruction (Fig. 4c).

3.5. Glacial termination V and MIS 11

Geochronologic constraints to the aggradation of the San Paolo Formation rely on three distinct outcrops in the Fosso Galeria stream valley (see map in Fig. 2b) and one outcrop at the Capitoline Hill in Rome (Karner and Renne, 1998; Karner and Marra, 1998; 2003). Results relate it to the deglaciation of T-5, which led into the MIS 11 interglacial. Thickness and stratigraphic features of the aggradational succession are shown in Fig. 6a, which merges data from the abovementioned outcrops with those from a section (San Cosimato, see Fig. 2b) that was previously described (Conato et al., 1980). The Capitoline Hill section reconstruction (see also Fig. 4a) integrates outcrop and borehole data (Corazza et al., 2004). The lower elevation of the base level of the San Paolo Formation at this location indicates that a significant tectonic drop has affected it. The tectonic displacement can be quantified by merging the Capitoline Hill data, where the top of the aggradational succession is eroded, with the stratigraphy of the INGV borehole in south-eastern Rome (Marra, 1999) (Fig. 6a'). There, the upper surface of the deposits of the San Paolo Formation is well preserved and geochronologically constrained by the 407 ± 3 ka pyroclastic-flow deposit of Pozzolane Nere (Marra et al., 2009). This reveals a tectonic lowering of 20–25 m (see Fig. 14 of Marra and Florindo, 2014), and gives an estimated thickness of ~ 40 m for the aggradational succession in Rome, consistent with that of the San Paolo Formation in Fosso Galeria (Fig. 6a–a'). The inferred tectonic displacement also affects the Vallerano lava plateau (Marra, 1999), dated 456 ± 5 ka (Marra et al., 2009), and is mostly sealed by the Tufo Lionato-Pozzolanelle pyroclastic-flow deposits at 356 ± 4 ka (Marra et al., 2009). The responsible faults are indicated in Fig. 4b.

Several dates were available for the San Paolo Formation already, falling in a range between 437 ± 8 and 410 ± 2 ka (Karner and Marra, 2003). Here, we have re-sampled the volcanoclastic layer at the base of the aggradational succession that is exposed at Pantano di Grano (see Fig. 3b), where a previous date of 437 ± 8 ka was reported based on three crystals. Our new sampling provided a larger, homogeneous population of six crystals, and yields an age of 438 ± 10 ka, supporting the non-reworked nature of the pyroclastic deposit (Fig. 6), and allowing us to calculate a better constrained, combined age of 437 ± 6 ka for this volcanic layer (Table 2). However, detailed investigation of the stratigraphic features of the San Paolo deposit at Pantano di Grano suggests that the gravel overlain by the pyroclastic deposit may be part of the older PG2 aggradational succession (Fig. 3a and 6a), related to an older deglaciation, rather than T-5 (possibly the MIS 18–17 transition; Marra et al., 1998). The pyroclastic deposit then occurs above a fluvial incision, likely related to the MIS 12 lowstand, and should pre-date aggradation of the San Paolo Formation (Fig. 6b). Preservation of this volcanoclastic layer suggests that the erosional (incision) process had ended by the time of its emplacement, in agreement with its age close to a minor, early peak of sea-level rise preceding T-5 (Fig. 6b).

The lowest pyroclastic layer within the fine-grained portion of the San Paolo aggradational succession yielded an age of 425 ± 5 ka (sample R94-30C). This is in close agreement with the age of the first, fast sea-level rise in T-5 in the sea-level reconstruction of Grant et al. (2014) (Fig. 6b).

4. Conclusions

We have chronologically constrained periods of aggradation of the Tiber River within the last half million years, using radioisotopic dating of intercalated volcanic deposits. Results are compared with the chronologically independently constrained Red Sea relative sea-level curve (Grant et al., 2014) and with the astronomi-

cally tuned $\delta^{18}\text{O}$ curve (Lisiecki and Raymo, 2005) (yellow bands in Fig. 7a and b, respectively).

Overall, we observe a good agreement between the timing of the Tiber's aggradational successions and intervals of fast sea-level rise documented by Grant et al. (2014), with one striking exception that concerns T-4, leading into MIS 9 (AU in Fig. 7a). For T-2 and T-5 we find particularly good agreement between documented sea-level rises and aggradation of the fine-grained portion of the so-called Epi-Tyrrhenian Formation (MIS 5) and San Paolo Formation (MIS 11), which is fully consistent with the especially well-dated sedimentary evidence for T-1. We also observe convincing evidence of aggradation in the Via Mascagni succession during MIS 8.5.

With respect to the apparent discrepancy noted for T-4, one possible explanation is that the documented aggradation represents an early phase, triggered by a smaller event in the sea-level record (Fig. 7a). However, the Aurelia Formation thickness would then suggest that the amplitude of this earlier sea-level rise may have been underestimated in the Red Sea reconstruction (Fig. 4). Also, this would imply that the aggradational succession corresponding with the major deglaciation of T-4 would not yet have been located at all in the study region, which is hard to reconcile with the extensive coverage of the fieldwork and borehole studies that have been undertaken. To address this problem, further work on the Aurelia Formation is needed for a broader regional investigation, including (if possible) more detailed age control, and precise assessments of the stratigraphic thicknesses. Equally, the chronologies of the Grant et al. (2014) Red Sea record, and for deep-sea benthic $\delta^{18}\text{O}$ records, should also be critically re-assessed for T-4.

Acknowledgements

We are grateful to Heather Stoll for useful suggestions and additional editing to the manuscript. We also thank one anonymous reviewer. This work contributes to the DTS-MIUR NextData project.

Appendix A. Supplementary material

Supplementary material related to this article can be found online at <http://dx.doi.org/10.1016/j.epsl.2016.05.037>.

References

- Alvarez, W., Ammerman, A.J., Renne, P.R., Karner, D.B., Terrenato, N., Montanari, A., 1996. Quaternary fluvial–volcanic stratigraphy and geochronology of the Capitoline hill in Rome. *Geology* 24, 751–754.
- Anzidei, A.P., Bulgarelli, G.M., Catalano, P., Cerilli, E., Gallotti, R., Lemorini, C., Milli, S., Palombo, M.R., Pantano, W., Santucci, E., 2012. Ongoing research at the late Middle Pleistocene site of La Polledrara di Cecanibbio (central Italy), with emphasis on humane elephant relationships. *Quat. Int.* 255, 171–187. <http://dx.doi.org/10.1016/j.quaint.2011.06.005>.
- Bellotti, P., Calderoni, G., Carboni, M.G., Di Bella, L., Tortora, P., Valeri, P., Zernitskaya, V., 2007. Late Quaternary landscape evolution of the Tiber River delta plain (Central Italy): new evidence from pollen data, biostratigraphy and ^{14}C dating. *Z. Geomorphol.* 51, 505–534.
- Belluomini, G., Iuzzolini, P., Manfra, L., Mortari, R., Zaffari, M., 1986. Evoluzione recente del delta del Tevere. *Geol. Rom.* 25, 213–234.
- Berger, A., 1978. Long-term variations of daily insolation and Quaternary climatic change. *J. Atmos. Sci.* 35, 2362–2367.
- Berger, W.H., Yasuda, M., Bickert, T., Wefer, G., Takayama, T., 1994. Quaternary timescale for the Ontong Java Plateau: Milankovitch template for Ocean Drilling Program Site 806. *Geology* 22, 463–467.
- Conato, V., Esu, D., Malatesta, A., Zarlenga, F., 1980. New data on the Pleistocene of Rome. *Quaternaria* 22, 131–176.
- Corazza, A., Lombardi, L., Marra, F., 2004. La geologia del Colle Capitolino. *Il Quaternario* 17 (2), 413–441.
- Florindo, F., Karner, D.B., Marra, F., Renne, P.R., Roberts, A.P., Weaver, R., 2007. Radioisotopic age constraints for Glacial Terminations IX and VII from aggradational sections of the Tiber River delta in Rome, Italy. *Earth Planet. Sci. Lett.* 256, 61–80. <http://dx.doi.org/10.1016/j.epsl.2007.01.014>.
- Grant, K.M., Rohling, E.J., Bar-Matthews, M., Ayalon, A., Medina-Elizalde, M., Ramsey, C.B., Satow, C., Roberts, A.P., 2012. Rapid coupling between ice volume and polar temperature over the past 150,000 years. *Nature* 491, 744–747.
- Grant, K.M., Rohling, E.J., Bronk Ramsey, C., Cheng, H., Edwards, R.L., Florindo, F., Heslop, D., Marra, F., Roberts, A.P., Tamisiea, M.E., Williams, F., 2014. Sea-level variability over five glacial cycles. *Nat. Commun.* 5, 5076. <http://dx.doi.org/10.1038/ncomms5076>.
- Grimaldi, S., 1998. Analyse technologique, chaîne opératoire et objectifs techniques. Torre in Pietra (Rome, Italie). *Paléo* 10, 109–122. <http://dx.doi.org/10.3406/pal.1998.1132>.
- Hays, J.D., Imbrie, J., Shackleton, N.J., 1976. Variations in the Earth's orbit: pacemaker of the ice ages. *Science* 194, 1121–1131.
- Huybers, P., 2006. Early Pleistocene glacial cycles and the integrated summer insolation forcing. *Science* 313, 508–511. <http://dx.doi.org/10.1126/science.1125249>.
- Imbrie, J., Hays, J.D., Martinson, D.G., McIntyre, A., Mix, A.C., Morley, J.J., Pisias, N.G., Prell, W.L., Shackleton, N.J., 1984. The orbital theory of Pleistocene climate: support from a revised chronology of the marine $\delta^{18}\text{O}$ record. In: Berger, et al. (Eds.), *Milankovitch and Climate*, vol. 1. Reidel Publishing Company, Dordrecht, Holland, pp. 269–305.
- Jicha, B.R., Rhodes, J.M., Singer, B.S., Michael, O.G., 2012. $^{40}\text{Ar}/^{39}\text{Ar}$ geochronology of submarine Mauna Loa volcano, Hawaii. *J. Geophys. Res.* 117, B09204. <http://dx.doi.org/10.1029/2012JB009373>.
- Karner, D.B., Marra, F., 1998. Correlation of fluviodeltaic aggradational sections with glacial climate history: a revision of the classical Pleistocene stratigraphy of Rome. *Geol. Soc. Am. Bull.* 110, 748–758.
- Karner, D.B., Marra, F., 2003. $^{40}\text{Ar}/^{39}\text{Ar}$ dating of Glacial Termination V and duration of the Stage 11 highstand. In: *Earth's Climate and Orbital Eccentricity: The Marine Isotope Stage 11 Question*. In: *Geophysical Monograph*, vol. 137. American Geophysical Union, pp. 61–66.
- Karner, D.B., Renne, P.R., 1998. $^{40}\text{Ar}/^{39}\text{Ar}$ geochronology of Roman province tephra in the Tiber River Valley: age calibration of Middle Pleistocene sea-level changes. *Geol. Soc. Am. Bull.* 110, 740–747.
- Karner, D.B., Marra, F., Florindo, F., Boschi, E., 2001a. Pulsed uplift estimated from terrace elevations in the coast of Rome: evidence for a new phase of volcanic activity? *Earth Planet. Sci. Lett.* 188, 135–148.
- Karner, D.B., Marra, F., Renne, P.R., 2001b. The history of the Monti Sabatini and Alban Hills volcanoes: groundwork for assessing volcanic–tectonic hazards for Rome. *J. Volcanol. Geotherm. Res.* 107, 185–215.
- Kuiper, K.F., Deino, A., Hilgen, F.J., Krijgsman, W., Renne, P.F., Wijbrans, J.R., 2008. Synchronizing rock clocks of Earth history. *Science* 320, 500–504. <http://dx.doi.org/10.1126/science.1154339>.
- Lisiecki, L.E., Raymo, M.E., 2005. A Pliocene–Pleistocene stack of 57 globally distributed benthic $\delta^{18}\text{O}$ records. *Paleoceanography* 20, PA 1003. <http://dx.doi.org/10.1029/2004PA001071>.
- Marino, G., Rohling, E.J., Rodríguez-Sanz, L., Grant, K.M., Heslop, D., Roberts, A.P., Stanford, J.D., Yu, J., 2015. Bipolar seesaw control on last interglacial sea level. *Nature* 522, 197–201. <http://dx.doi.org/10.1038/nature14499>.
- Marra, F., 1999. Low-magnitude earthquakes in Rome: structural interpretation and implications for local stress-field. *Geophys. J. Int.* 138, 231–243.
- Marra, F., Florindo, F., 2014. The subsurface geology of Rome: sedimentary processes, sea-level changes and astronomical forcing. *Earth-Sci. Rev.* 136, 1–20.
- Marra, F., Florindo, F., Karner, D.B., 1998. Paleomagnetism and geochronology of early Middle Pleistocene depositional sequences near Rome: comparison with the deep sea $\delta^{18}\text{O}$ climate record. *Earth Planet. Sci. Lett.* 159, 147–164.
- Marra, F., Florindo, F., Boschi, E., 2008. The history of glacial terminations from the Tiber River (Rome): insights to glacial forcing mechanisms. *Paleoceanography* 23, PA2205. <http://dx.doi.org/10.1029/2007PA001543>.
- Marra, F., Karner, D.B., Freda, C., Gaeta, M., Renne, P.R., 2009. Large mafic eruptions at the Alban Hills Volcanic District (Central Italy): chronostratigraphy, petrography and eruptive behavior. *J. Volcanol. Geotherm. Res.* 179, 217–232. <http://dx.doi.org/10.1016/j.jvolgeores.2008.11.009>.
- Marra, F., Bozzano, F., Cinti, F.R., 2013. Chronostratigraphic and lithologic features of the Tiber River sediments (Rome, Italy): implications on the post-glacial sea-level rise and Holocene climate. *Glob. Planet. Change* 107, 157–176. <http://dx.doi.org/10.1016/j.gloplacha.2013.05.002>.
- Marra, F., Pandolfi, L., Petronio, C., Di Stefano, G., Gaeta, M., Salari, L., 2014. Reassessing the sedimentary deposits and vertebrate assemblages from Ponte Galeria area (Roma, central Italy): an archive for the Middle Pleistocene faunas of Europe. *Earth-Sci. Rev.* 139, 104–122.
- Marra, F., Ceruleo, P., Jicha, B., Pandolfi, L., Petronio, C., Salari, L., 2015. A new age within MIS 7 for the Homo neanderthalensis of Saccopastore in the glacio-eustatically forced sedimentary successions of the Aniene River Valley, Rome. *Quat. Sci. Rev.* 129, 260–274. <http://dx.doi.org/10.1016/j.quascirev.2015.10.027>.
- Milankovitch, M., 1941. *Kanon der Erdbestrahlung und Seine Anwendung auf das Eiszeitenproblem*, vol. 133. Akad. R. Serbie, Belgrade, 633 pp.
- Milli, S., 1997. Depositional setting and high-frequency sequence stratigraphy of the Middle–Upper Pleistocene to Holocene deposits of the Roman basin. *Geol. Rom.* 33, 99–136.

- Milli, S., Moscatelli, M., Palombo, M.R., Parlagreco, L., Paciucci, M., 2008. Incised valleys, their filling and mammal fossil record: a case study from Middle–Upper Pleistocene deposits of the Roman Basin (Latium, Italy). In: Amorosi, A., Haq, B.U., Sabato, L. (Eds.), *Advances in Application of Sequence Stratigraphy in Italy*. *GeoActa* 1, 667–687. Special Publication.
- Muller, R.A., MacDonald, G.J., 1997. Glacial cycles and astronomical forcing. *Science* 277, 215–218. <http://dx.doi.org/10.1126/science.277.5323.215>.
- Nomade, S., Renne, P.R., Vogel, N., Deino, A.L., Sharp, W.D., Becker, T.A., Jaouni, A.R., Mundil, R., 2005. Alder Creek sanidine (ACs-2): a Quaternary $^{40}\text{Ar}/^{39}\text{Ar}$ dating standard tied to the Cobb Mountain geomagnetic event. *Chem. Geol.* 218, 315–338.
- Nomade, S., Guillou, H., Bahain, J.J., Peretto, C., Piperno, M., Falguères, C., Voinchet, P., Arzarello, M., Scao, V., Bulgarelli, G.M., Anzidei, A.P., 2014. La datation $^{40}\text{Ar}/^{39}\text{Ar}$ ($^{40}\text{K}/^{40}\text{Ar}$): applications à la paléontologie et en archéologie. In: *Abstract Book, XVII World UISPP Congress, Burgos, 1–7 September 2014*.
- Paillard, D., 1998. The timing of Pleistocene glaciations from a simple multiple-state climate model. *Nature* 391, 378–391.
- Paillard, D., 2015. Quaternary glaciations: from observations to theories. *Quat. Sci. Rev.* 107, 11–25. <http://dx.doi.org/10.1016/j.quascirev.2014.10.002>.
- Phillips, D., Matchan, E.L., 2013. Ultra-high precision $^{40}\text{Ar}/^{39}\text{Ar}$ ages for Fish Canyon Tuff and Alder Creek Rhyolite sanidine: new dating standards required? *Geochim. Cosmochim. Acta* 121, 229–239. <http://dx.doi.org/10.1016/j.gca.2013.07.003>.
- Raymo, M.E., Lisiecki, L.E., Nisancioglu, K.H., 2006. Plio–Pleistocene ice volume, Antarctic Climate, and the Global $\delta^{18}\text{O}$ record. *Science* 313, 492–495.
- Renne, P.R., Swisher, C.C., Deino, A.L., Karner, D.B., Owens, T.L., DePaolo, D.J., 1998. Intercalibration of standards, absolute ages and uncertainties in $^{40}\text{Ar}/^{39}\text{Ar}$ dating. *Chem. Geol.* 145, 117–152. [http://dx.doi.org/10.1016/S0009-2541\(97\)00159-9](http://dx.doi.org/10.1016/S0009-2541(97)00159-9).
- Renne, P.R., Balco, G., Ludwig, K.R., Mundil, R., Min, K., 2011. Response to the comment by W.H. Schwarz et al. on “Joint determination of ^{40}K decay constants and $^{40}\text{Ar}/^{40}\text{K}$ for the Fish Canyon sanidine standard, and improved accuracy for $^{40}\text{Ar}/^{39}\text{Ar}$ geochronology” by P.R. Renne et al. *Geochim. Cosmochim. Acta* 75, 5097–5100. <http://dx.doi.org/10.1016/j.gca.2011.06.021>.
- Rivera, T.A., Storey, M., Schmitz, M.D., Crowley, J.L., 2013. Age intercalibration of $^{40}\text{Ar}/^{39}\text{Ar}$ sanidine and chemically distinct U/Pb zircon populations from the Alder Creek Rhyolite Quaternary geochronology standard. *Chem. Geol.* 345, 87–98.
- Rohling, E.J., Grant, K., Bolshaw, M., Roberts, A.P., Siddall, M., Hemleben, Ch., Kucera, M., 2009. Antarctic temperature and global sea level closely coupled over the past five glacial cycles. *Nat. Geosci.* 2, 500–504. <http://dx.doi.org/10.1038/NGE0557>.
- Shackleton, N.J., Berger, A., Peltier, W.R., 1990. An alternative astronomical calibration of the Lower Pleistocene timescale based on ODP site 677. *Trans. R. Soc. Edinb. Earth Sci.* 81, 251–261.
- Sorgi, C., 1994. La successione morfo-litostratigrafica in destra Tevere dell'ambito dell'evoluzione geologica quaternaria dell'area romana. Unpublished “Tesi di Laurea”, Università degli Studi di Roma “La Sapienza”.
- Stanford, J.D., Hemingway, R., Rohling, E.J., Challenor, P.G., Medina-Elizalde, M., Lester, A.J., 2011. Sea-level probability for the last deglaciation: a statistical analysis of far-field records. *Glob. Planet. Change* 79, 193–203. <http://dx.doi.org/10.1016/j.gloplacha.2010.11.002>.
- Steiger, R.H., Jäger, E., 1977. Subcommision on geochronology: convention on use of decay constants in geo- and cosmochronology. *Earth Planet. Sci. Lett.* 36, 359–362.
- Tziperman, E., Gildor, H., 2003. On the mid-Pleistocene transition to 100-kyr glacial cycles and the asymmetry between glaciation and deglaciation times. *Paleoceanography* 18.